Thermal behaviour and kinetics of coal/biomass blends during co-combustion

M.V. Gil, D. Casal, C. Pevida, J.J. Pis, F. Rubiera*

Instituto Nacional del Carbón, CSIC, Apartado 73, 33080 Oviedo, Spain

Abstract

The thermal characteristics and kinetics of coal, biomass (pine sawdust) and their blends were evaluated under combustion conditions using a non-isothermal thermogravimetric method (TGA). Biomass was blended with coal in the range of 5-80 wt% to evaluate their co-combustion behaviour. No significant interactions were detected between the coal and biomass, since no deviations from their expected behaviour were observed in these experiments. Biomass combustion takes place in two steps: between 200-360 ºC the volatiles are released and burned, and at 360-490 ºC char combustion takes place. In contrast, coal is characterized by only one combustion stage at 315-615 ºC. The coal/biomass blends presented three combustion steps, corresponding to the sum of the biomass and coal individual stages. Several solid-state mechanisms were tested by the Coats-Redfern method in order to find out the mechanisms responsible for the oxidation of the samples. The kinetic parameters were determined assuming single separate reactions for each stage of thermal conversion. The combustion process of coal consists of one reaction, whereas, in the case of the biomass and coal/biomass blends, this process consists of two or three independent reactions, respectively. The results showed that the chemical first order reaction is the most effective mechanism for the first step of

* Corresponding author. Tel.: +34 985 118 975; Fax: +34 985 297 662.

E-mail address: frubiera@incar.csic.es (F. Rubiera)

biomass oxidation and for coal combustion. However, diffusion mechanisms were found to be responsible for the second step of biomass combustion.

Keywords: Biomass; Coal; Co-combustion; TG; Kinetics

1. Introduction

Recent awareness of CO_2 emissions has resulted in a shift from less environmentally friendly fossil fuels to renewable and sustainable energy alternatives. Among these, biomass is considered to be one of the few viable replacement options (Munir et al., 2009). Biomass can be grown in a sustainable way through a cyclical process of fixation and release of CO_2, thereby mitigating global warming problems (McKendry, 2002). Biomass fixes CO_2 in the form of lignocellulosics during photosynthesis, and the CO_2 emitted from the combustion of these materials makes no net contribution to the accumulation of CO_2 in the atmosphere or to the greenhouse effect.

Many technologies have been studied in recent years for their possible use with biomass, such as combustion, pyrolysis, gasification, liquefaction, etc. Co-combustion is also one of the most promising options for application with renewable fuels. There are several reasons to blend biomass with coal or with other types of fuel prior to burning. The co-combustion of coal/biomass blends will help to reduce the consumption of fossil fuels. Sometimes biofuel products are mixed with coal to achieve better control of the burning process (Wang et al., 2009). In co-combustion processes, a volatile matter content greater than 35% is sought in order to provide a stable flame (Biagini et al., 2002), which could be attained by using biomass. The ash deposition and fouling problems on hot surfaces, which are commonly encountered in the combustion of

biomass can be reduced or altogether eliminated by burning coal/biomass blends (Haykiri-Acma and Yaman, 2008). Furthermore, existing coal-fuelled power plants may continue to be used with very few modifications (Biagini et al., 2002), and as a final argument, the co-utilization of biomass or waste in existing coal-fired plants is likely to result in a number of environmental, technical and economical benefits (Kastanaki and Vamvuka, 2006).

Thermogravimetric analysis (TGA) is one of the most common techniques used to rapidly investigate and compare thermal events and kinetics during the combustion and pyrolysis of solid raw materials, such as coal, woods, etc. (Pis et al., 1996; Rubiera et al., 1997; Haykırı-Açma, 2003; Skodras et al., 2007; Wang et al., 2009). It is able to measure the mass loss of a sample as a function of time and temperature. The temperatures at which combustion or decomposition reactions in the sample start can also be followed by TGA. Moreover, quantitative methods can be applied to TGA curves in order to obtain kinetic parameters, and the kinetics of the thermal events can be determined by applying the Arrhenius equation to the separate slopes of constant mass loss (Zhou et al., 2006; Shen et al., 2009; Wang et al., 2009).

Cumming and McLaughlin (1982) indicated that the information obtained from TGA combustion profiles can be used for an initial evaluation of the combustion behaviour at industrial scale. TGA techniques operate at different conditions to those encountered in a pulverised coal combustor. Other bench equipment such as drop tube furnaces and entrained flow reactors simulate more closely the combustion conditions of industrial pf combustors. However, since the pilot- and full-scale tests are costly to operate, the above techniques can help in the understanding of coal combustion behaviour. Although extrapolation to other devices at larger scale cannot be performed directly,

thermogravimetric analysis is very useful from a fundamental viewpoint, and for comparison between samples (Arenillas et al., 2004; Rubiera et al., 2002).

A knowledge of the thermal characteristics of biomass and of biomass combustion kinetics is essential for understanding and modelling combustion in furnaces at industrial scale, both in the case of co-firing with coal or alone (Munir et al., 2009). Such a knowledge is also necessary for the design and operation of conversion systems (Cai et al., 2008). According to Shen et al. (2009), a good understanding of the decomposition of biomass during thermochemical conversion is important for developing an efficient processing technology. Most studies related to the kinetics of biomass decomposition are focused on pyrolysing these materials under inert atmospheres. However, the most recent research has been directed towards the study of biomass decomposition in oxidative environments (Safi et al., 2004; Shen et al., 2009; Yorulmaz and Atimtay, 2009), a subject about which information is still scarce.

The aim of this work is to compare the thermal properties and kinetic behaviour of coal, pine sawdust and their blends in an oxidative atmosphere using a thermogravimetric analyzer in order to investigate the combustion characteristics of coal/biomass blends.

2. Materials and methods

2.1. Experimental setup

The feedstock materials used in this work were a high-volatile bituminous coal and pine sawdust. The samples were collected from the Aboño Power Plant located in Asturias (Spain), where co-combustion trials are currently being conducted. Ultimate and proximate analyses together with the heating values of the coal and pine samples are presented in Table 1. Different mixtures of both materials were prepared. These

included 5, 10, 20, 50 and 80 wt% of pine sawdust (5P95C, 10P90C, 20P80C, 50P50C and 80P20C, respectively). The raw materials are named 100C (coal) and 100P (pine sawdust). First, the samples were ground and sieved in order to obtain a particle size fraction of 75-150 μm. The coal/pine mixtures were mixed in appropriate proportions and manually homogenised.

The techniques employed in this study were thermogravimetric analysis (TG) and derivative thermogravimetry (DTG). Non-isothermal TGA was performed using a Setaram TAG24 analyser. The analyses were carried out under a 50 cm^3 min^{-1} air flow at a heating rate of 15 ºC min^{-1} from room temperature to 1000 ºC. Approximately 5 mg of sample was used for each experiment and it was dispersed flatly on a crucible, which had a flat bottom 8 mm in diameter and 3 mm in depth,. A small amount of sample and a slow heating rate were used to avoid heat transfer limitations and to minimize mass transfer effects. Duplicate experiments for each test were performed in order to test the reproducibility of the results. The mass loss (TG) and derivative curves (DTG) of the samples were represented as a function of temperature.

In order to find out whether interactions between the components of the blends occurred, the theoretical DTG curves of the blends were calculated as the sum of the decomposition curves of each individual component. Thus:

$$(\mathrm{d}m/\mathrm{d}t) = x_1(\mathrm{d}m/\mathrm{d}t)_{\mathrm{coal}} + x_2(\mathrm{d}m/\mathrm{d}t)_{\mathrm{biomass}}$$

where $(\mathrm{d}m/\mathrm{d}t)_{\mathrm{coal}}$ and $(\mathrm{d}m/\mathrm{d}t)_{\mathrm{biomass}}$ are the mass loss rates of the individual fuels and x_1, x_2 are the proportions of coal and biomass in the blend, respectively.

2.2. Kinetic analysis

The thermal devolatilisation curve is usually obtained as a sum of the contributions of the corresponding individual components (Heikkinen et al., 2004). However, combustion is a more complex process, since the presence of oxygen generates a variety of additional phenomena (Skodras et al., 2007). These include the appearance of gas-phase reactions between the volatiles released at low temperatures and oxygen, and the combustion of the char generated in the early stages of the solids degradation (Bilbao et al., 1997).

A two-stage reaction kinetics scheme consisting of two independent reactions is proposed for the thermal decomposition of the biomass under an oxidative atmosphere (Liu et al., 2002; Shen et al., 2009), represented by the DTG curves. The kinetic scheme includes the two separate reactions:

A (solid) → B (char) + C1 (gas) (first stage)

B (char) → C2 (gas) + D (ash) (second stage)

The approach used in the present work to calculate the kinetic parameters was based on the Arrhenius equation, which has been used by other researchers in order to obtain kinetic parameters of thermal events under combustion conditions (Munir et al., 2009; Shen et al., 2009; Wang et al., 2009; Yorulmaz and Atimtay, 2009). These two separate reactions are thought to be governed by the first-order Arrhenius law and so, the kinetics of the reaction is described as:

$$dx/dt = k\,f(x) \quad (1)$$

$$k = A\exp(-E/RT) \quad (2)$$

where $f(x)$ represents the hypothetical model of the reaction mechanism, k is the reaction rate, A the pre-exponential factor (min^{-1}), E the activation energy (kJ mol^{-1}), R the gas

constant (8.314 J K^{-1} mol^{-1}), T the absolute temperature (K), t the time (min) and x the loss in mass fraction or mass conversion ratio, which can be calculated by the following relationship:

$$x = (m_0 - m_t)/(m_0 - m_f) \quad (3)$$

where m_0 is the initial mass of the sample, m_t the mass of the sample at time t and m_f the final mass of the sample.

For a constant heating rate β (K min^{-1}) during combustion, $\beta = dT/dt$, Eq. (1) can be transformed into:

$$dx/f(x) = (k/\beta)\, dT \quad (4)$$

Integrating Eq. (4) gives:

$$g(x) = \int_0^x dx / f(x) = A/\beta \int_{T_0}^{T} \exp(-E/RT) dT \quad (5)$$

where $g(x)$ is the integral function of conversion.

Eq. (5) is integrated by using the Coats-Redfern method (Coats and Redfern, 1964), yielding:

$$\ln[g(x)/T^2] = \ln[AR/\beta E(1-2RT/E)] - E/RT \quad (6)$$

Since it can be demostrated that for most values of E and for the temperature range of combustion, the expression $\ln[AR/\beta E(1-2RT/E)]$ in Eq. (6) is essentially constant (Zhou et al., 2006), if $\ln[g(x)/T^2]$ is plotted versus $1/T$, a straight line should be obtained. Moreover, if the correct $g(x)$ is used, the plot of $\ln[g(x)/T^2]$ against $1/T$ should give a straight line with a high correlation coefficient of linear regression analysis, from which the values of E and A can be derived. The activation energy, E, can be calculated from the slope of the line, $-E/R$; and by taking the temperature at which $m_t = (m_0 + m_f)/2$ as the intercept term of Eq. (6), the pre-exponential factor A can also be calculated (Zhou et al., 2006).

The function *g(x)*, or *f(x*), depends on the mechanism controlling the reaction and the size and shape of the reacting particles. Table 2 shows the expressions of *g(x)* for the basic model functions usually employed for the kinetic study of solid state reactions. By means of these functions it was possible to estimate the reaction mechanisms governing the process of thermal oxidation of the samples from the TG curves. The form of *g(x)* that gives a straight line with the highest correlation coefficient will be considered the function of the model that best represents the kinetics of mass loss for each separate reaction.

In most dynamic studies that use TGA, the first-order chemical reaction assumption (O1 model) is the most frequently used. In addition to this reaction mechanism, other chemical reactions (O2 and O3 models), boundary controlled reactions (R2 and R3 models) and diffusion mechanisms (D1, D2, D3 and D4 models) are commonly applied to describe the combustion reactions of biomass.

3. Results and discussion

3.1. Thermal characteristics of the samples under air atmosphere

The biomass, pine sawdust (100P), has less fixed carbon and more volatiles than the coal, 100C, and it also has a lower ash content and a negligible sulphur content (Table 1). These characteristics favour clean combustion conditions (Vamvuka et al., 2003b). The nitrogen content in the biomass is low, and therefore, emissions of nitrogen oxides from this element will probably be minimal. In comparison with coal, biomass contains a higher proportion of oxygen and hydrogen and less carbon (Table 1), which reduces its heating value because the amount of energy contained in carbon-oxygen and carbon-hydrogen bonds is lower than in carbon-carbon bonds (Munir et al., 2009). However,

the higher oxygen content in the biomass indicates that it will have a higher thermal reactivity than coal (Haykiri-Acma and Yaman, 2008).

Biomass typically has a volatile matter/fixed carbon (VM/FC) ratio of > 4.0, while the VM/FC ratio for coal is almost always <1.0 (Tillman, 2000). In this work, the VM/FC ratio for the biomass is approximately 5.0 and for the coal 0.5. Thus, for biomass fuels, the predominant form of combustion will take place via the gas-phase oxidation of the volatile species (Wang et al, 2009).

The experimental DTG curves for the coal and pine sawdust samples and their blends, under air atmosphere, are shown in Fig. 1. In this figure, the curves of the blends are situated between those of the individual fuels. Before ignition, some increase in mass may occur due to the chemisorption of oxygen (Haykiri-Acma and Yaman, 2008), as can be observed from the negative values of the DTG curves of coal sample (100C) and the samples with a high percentage of coal (5P95C, 10P90C and 20P80C).

From the DTG curves (Fig. 1), it can be seen that an initial mass loss (stage A) occurred between the temperatures of 25 ºC and 105 ºC for all samples, due to moisture evaporation. After that, two-step mass losses (stages B and C) took place in biomass sample, 100P, compared to only a one-step mass loss (stage D) for coal sample, 100C. Stage B would be due to the release of volatiles and their combustion, and stage C would be due to the char oxidation. However, all the coal/biomass blends displayed three step mass losses (stages B, C and D). In the case of the blends, the first two mass losses, stages B and C, were mainly due to the burning of biomass, whereas the last one (stage D) was mostly due to the combustion of coal. However, part of the mass loss is due to the coal because the second peak of the biomass (stage C) and the peak of the

coal (stage D) clearly overlap. Similarly, some of the mass loss of stage D is due to the biomass.

Table 3 shows the temperature ranges for the three different regions of mass loss after the initial loss of moisture during the combustion of the samples, the mass loss produced in each of these regions and the final residue after combustion. The initial temperature in stage B and the final temperature in stage D were taken as the temperature values at which the rate of mass loss was 0.005 % s^{-1} (Rubiera et al., 1999). The coal (100C) starts to devolatilise at a higher temperature compared to the biomass (100P), 316 ºC and 196 ºC respectively. Stages C and D occur in a range of temperatures that are similar in all the samples, which suggests that the blending process does not affect the combustion behaviour of the individual components. However, the initial temperature of stage B decreased as the percentage of biomass increased, suggesting that combustion was brought forward due to the formation of volatiles from the biomass. Indeed, the biomass has a much higher volatile matter content than the coal (Table 1), which causes it to burn at lower temperatures.

The mass loss from biomass (100P) is higher than in other samples in stage B, in the 200-350 ºC temperature range (Table 3). However, in stage D, above approximately 480 ºC, the mass loss from the biomass is over and the mass loss from coal (100C) is now higher than from the blends. The mass losses corresponding to the blends lie between those of the individual fuels. The mass loss in stage B increases with the biomass content due to the much higher volatile matter content of the biomass (Table 1). Similarly, the mass loss in stage D increases as the coal content of the blend increases, due to the higher amount of char in the coal.

In the case of the biomass, the mass loss in stage B is due to oxidative degradation –i.e. volatiles are released and then burned–, whereas the mass loss in stage C is due to the combustion of char. Haykırı-Açma (2003) described this first stage as the burning region in which volatiles are released and burned. Zheng and Koziński (2000) reported that biomass combustion consisted of two main steps, the first characterised by the devolatilization process and burning of the released light organic volatiles, and the second resulting from the oxidation of char. Liu et al. (2002) added that the first DTG peak in air is largely due to the pyrolysis of hemicellulose and cellulose, but also partly due to that of lignin, while the second DTG peak is largely caused by oxidation.

Table 4 shows the peak temperatures and the maximum rates of mass loss for the three stages after the initial loss of moisture during the combustion of all the samples. The maximum rate of mass loss is considered directly proportional to the reactivity of the sample (Zheng and Koziński, 2000). In stage B, the maximum mass loss rate increases with the percentage of biomass present in the blend, which suggests that the higher the amount of biomass in the blend, the faster the rate of mass loss between 200-350 ºC or, in other words, the higher the reactivity of the samples in this range. This indicates that a greater number of volatiles are formed and that they ignite at these temperatures due to the presence of biomass in the blends. In stage C, this is not the case because of the overlapping of the C and D stages. However, for biomass (100P), the maximum rate of mass loss in stage C is lower than that of stage B, a finding also reported by Ghaly et al. (1993) for straw samples. In stage D, which is due to the presence of coal, the maximum rate of mass loss increases with the rise in the percentage of coal in the blend, indicating that the higher the amount of coal in the blend, the faster the mass loss in the 350-

600 ºC temperature range. This is due to the fact that coal has a higher carbon content (Table 1).

The temperature value at the maximum rate of mass loss is usually considered inversely proportional to the reactivity and combustibility of the sample (Haykırı-Açma, 2003). In relation to the B and D stages, no significant variation is observed between the different samples (Table 4). However, in the C region, a decrease in the peak temperature can be observed with the increase in the percentage of pine sawdust in the blend, reflecting the higher reactivity of the biomass.

3.2. Interactions between the components of the blends

No significant deviations were observed between the experimental and theoretical DTG curves of the coal/sawdust blends, as can be seen in Fig. 1. Therefore, according to the DTG results, no interactions between the components of the blends occurred, reflecting the additive behaviour of the coal/biomass blends and the absence of synergetic effects during the combustion process. Several authors, however, have observed interactions between the components of coal/biomass blends (Zhou et al., 2006; Skodras et al., 2007), while others have reported the additive behaviour of coal and biomass blends (Biagini et al., 2002; Kastanaki et al., 2002; Vamvuka et al., 2003a, b; Sadhukhan et al., 2008). It should be pointed out, however, that none of these studies were carried out under combustion conditions but during pyrolysis experiments. Fitzpatrick et al. (2009) studied the co-combustion of coal and pine wood in a fixed bed combustor and they observed synergy in organics emissions from the coal/pine blends, with lower emissions than would be expected on an additive basis. However, it has to be considered that in

fixed bed combustion, the particles are larger and they would be close together and synergistic effects would be therefore observed.

In this work, the absence of any interaction indicates that the combustion reactions of biomass or coal are not significantly affected by the presence of coal or biomass respectively. Each component of the mixture behaves independently and does not interact with the other materials in the experiments carried out with blends of pine sawdust and coal under the conditions established in this study.

3.3. Kinetic parameters

Several solid-state mechanisms (Table 2) were tested by the Coats-Redfern method in order to determine the mechanisms responsible for the oxidation of the samples under study. The kinetic parameters were determined assuming single separate reactions for a particular stage of thermal conversion. According to the DTG plot (Fig. 1), a single reaction could be used to describe the coal (100C) combustion process, whereas for biomass (100P) and the coal/biomass blends (5P95C to 80P20C), two or three independent reactions, respectively, are necessary. Thus, Eq. (6) was applied separately to each of the stages, and the conversion, x, was recalculated for each reaction. The form of $g(x)$ which gives a straight line with the highest correlation coefficient will be considered to be the function of the model that best represents the kinetic mass loss for each separate reaction. Fig. 2 shows the plots of $\ln[g(x)/T^2]$ against $1/T$ that gave the highest correlation coefficient values for all samples. From the slope of each line, the values of E and A were obtained.

The mechanisms that yielded the highest thermal kinetics correlation coefficient are shown in Table 5, where R^2 represents their correlation coefficients. The high

coefficient values indicate that the corresponding reaction model satisfactorily fitted the experimental data. Table 5 also shows the values of activation energy, *E*, and pre-exponential factor, *A*, for the three stages (B, C and D) for all the samples, each of which was obtained employing the most suitable model.

The solid-state reaction follows the first-order kinetics model (O1) when the rate-determining step is the chemical reaction. In phase boundary controlled reactions, the reaction is controlled by the movement of an interface at constant velocity and the reaction occurs almost instantaneously, with the result that the surface of each particle is covered with a layer of the product. R2 is a function used for a circular disc reacting from the edge inward, whereas R3 is used for a sphere which reacts from the surface inward. This mechanism is sometimes assumed to be the governing conversion model in the combustion of some carbonaceous materials (López-Fonseca et al., 2006). In a diffusion-controlled reaction, D1 is the function for a one-dimensional diffusion process governed by a parabolic law, with a constant diffusion coefficient. For diffusion in cylinders or spheres, it is necessary that all three dimensions be taken into account. D2 is the function for a two-dimensional diffusion-controlled process in a cylinder. D3 is Jander's equation for diffusion-controlled solid-state reaction kinetics in a sphere, where diffusion in all three directions is all-important. D4 is Ginstling-Brounshtein's equation for a diffusion-controlled reaction starting from the outside of a spherical particle (Alshehri et al., 2000). In a diffusion-controlled reaction, numerous chemical reactions or micro-structural changes in solids take place through solid-state diffusion, i.e., the movement and transport of gas molecules in the solid phase (Yorulmaz and Atimtay, 2009).

For stage B, models O2, O3 and D1 showed correlation coefficients between 0.9186 and 0.9890 for all the samples studied (data not shown). On the other hand, models R2, R3, D2, D3 and D4 had higher correlation coefficients, between 0.9879 and 0.9968 (data not shown). However, model O1 showed the highest correlation coefficients for all the samples with values exceeding 0.9973 (Table 5).

For stage C, models O2 and O3 showed correlation coefficients between 0.8738 and 0.9437 for all the samples studied. Model D1 presented even higher correlation coefficients, between 0.9820 and 0.9942, while models O1, R2, R3 and D2 exhibited correlation coefficients between 0.9940 and 0.9978. None of these models or their results have been included in Table 5. However, models D3 and D4 had the highest correlation coefficients, with values higher than 0.9980 (Table 5).

Finally, for stage D, models O2 and O3 showed correlation coefficients between 0.9178 and 0.9511 for all the samples studied (data not shown). Models R2, R3, D1, D2, D3 and D4 displayed correlation coefficients between 0.9427 and 0.9723 for all the samples of coal/biomass blends (data not shown). For the coal sample (100C), all the models, except O2 and O3, presented correlation coefficients higher than 0.99 (data not shown), with model O1 showing the highest value, equal to 0.9986 for this sample (Table 5). Model O1 also presented the highest correlation coefficients for the coal/biomass blends, > 0.9921 (Table 5).

Thus, the results confirm that the chemical first order reaction (O1 model) is the most effective solid-state mechanism for the first step of biomass oxidation (stage B) and for coal combustion (stage D). However, diffusion mechanisms (D3 and D4) were found to be responsible for the second step of biomass combustion (stage C).

The use of thermal analysis in order to find the mechanism responsible for the oxidation process may result in more than one equation fitting the experimental results. Therefore, a combination of TG analysis with dynamic and isothermal studies could be employed to determine the exact mechanisms and thermal constants of the oxidation processes (Yorulmaz and Atimtay, 2009).

As regards the kinetic parameters, the pre-exponential factor, *A*, is more closely related with material structure, whereas the reactivity of samples is determined by the activation energy, *E*, (Yorulmaz and Atimtay, 2009). The activation energy, *E*, in the first stage (stage B) of the biomass sample (100P) showed a value equal to 102 kJ mol^{-1} (Table 5), which is similar to the values recorded by Shen et al. (2009) in the first stage of the oxidation of their biomass samples (104-125 kJ mol^{-1}). These authors found higher values for *E* in the second stage of the oxidation process under low heating rates (150-220 kJ mol^{-1}). In the present study, the activation energy in stage C for the biomass (100P) was 219-236 kJ mol^{-1}. The *E* values observed by Liu et al. (2002) reached 52-99 kJ mol^{-1} for the first stage of oxidation and 87-202 kJ mol^{-1} for the second stage with leaf and wood samples. For beech and Douglas fir, Branca and Di Blasi (2004) found global *E* values ranging between 106-226 kJ mol^{-1}. Wang et al. (2009) found values of 88-115 kJ mol^{-1} for the first stage of oxidation and 153-210 kJ mol^{-1} for the second stage with wheat straw and coal and wheat straw mixtures.

Table 5 shows that for stage B, the calculated values of *E* and *A* (model O1) for biomass sample (100P) were lower than those calculated for the blends with a coal content of more than 50%, increasing as the coal percentage increased. This shows that the addition of pine sawdust to coal facilitates the volatilization and gaseous phase combustion processes at low temperatures, since lower activation energies are sufficient

for the processes to develop, which is in agreement with the decrease in the initial temperature of stage B as the percentage of biomass increases. Reactions with a high activation energy require a high temperature or a longer reaction time (Lázaro et al., 1998). The blends with 50 and 80 wt% of biomass (50P50C and 80P20C) presented similar *E* and *A* values to that of the pure biomass (100P). Thus, in these cases the presence of coal does not significantly affect combustion during this first stage. When the coal percentage is 80% (20P80C), the influence of coal during stage B is small, since the values of *E* and *A* are only slightly higher. But when the percentage of coal is higher than 80% (5P95C and 10P90C), significantly greater values of *E* and *A* are observed in this first stage.

For stage D, where only coal is present, the values of *E* and *A* (model O1) corresponding to the coal sample (100C) were lower than all the other values (Table 5). However, these values increased with the increase in biomass content. When the percentage of biomass is 5-20% (5P95C, 10P90C and 20P80C), the values of *E* and *A* are only slightly higher than those of coal. However, when the percentage of biomass is higher, greater values of *E* and *A* are observed.

For stage C, the calculated values of *E* and *A* (models D3 and D4) were found to be consistently higher than those of the other stages (Table 5), but fairly similar to each other, both in the case of the biomass and the blends. This indicates that the char combustion stage requires a higher activation energy than the devolatilisation stage.

5. Conclusions

Pine sawdust was subjected to two combustion steps: between 200-360 ºC, when the volatiles were released and burned, and between 360-490 ºC, when char combustion

occurred. However, coal was subjected to only one combustion step: between 315-615 ºC. The coal/biomass blends experienced all three combustion steps. When the biomass percentage in the blend was 50 wt% or more, devolatilisation was the predominant process. No synergistic effect during coal and biomass co-combustion was observed in these experiments. The combustion process of coal consists of one reaction, whereas, for biomass and the coal/biomass blends, the process consists of two or three independent reactions, respectively. The results of the kinetic analysis showed that the O1 mechanism (first-order chemical reaction) was assumed to be the main mechanism responsible for the first stage of biomass oxidation and for coal combustion. On the other hand, D3 and D4 diffusion mechanisms were observed to be the controlling mechanisms in the second stage of biomass combustion.

Acknowledgements

Work carried out with financial support from the Spanish MICINN (Project PS-120000-2006-3, EcoCombos), and co-financed by the European Regional Development Fund, ERDF.

References

Alshehri, S.M., Monshi, M.A.S., Abd El-Salam, N.M., Mahfouz, R.M., 2000. Kinetics of the thermal decomposition of γ-irradiated cobaltous acetate. Thermochim. Acta 363, 61-70.

Arenillas, A., Rubiera, F., Arias, B., Pis, J.J., Faúndez, J.M., Gordon, A.L., García, X.A., 2004. A TG/DTA study on the effect of coal blending on ignition behaviour. J. Therm. Anal. Calorim. 76, 603-614.

Biagini, E., Lippi, F., Petarca, L., Tognotti, L., 2002. Devolatilization rate of biomasses and coal-biomass blends: an experimental investigation. Fuel 81, 1041-1050.

Bilbao, R., Mastral, J.F., Aldea, M.E., Ceamanos, J., 1997. Kinetic study for the termal decomposition of cellulose and pine sawdust in an air atmosphere. J. Anal. Appl. Pyrol. 39, 53-64.

Branca, C., Di Blasi, C., 2004. Global intrinsic kinetics of wood oxidation. Fuel 83, 81-87.

Cai, J., Wang, Y., Zhou, L., Huang, Q., 2008. Thermogravimetric analysis and kinetics of coal/plastic blends during co-pyrolysis in nitrogen atmosphere. Fuel Process. Technol. 89, 21-27.

Coats, A.W., Redfern, J.P., 1964. Kinetic parameters from thermogravimetric data. Nature 201, 68-69.

Cumming, J.W., McLaughlin, J., 1982. The thermogravimetric behaviour of coal. Thermochim. Acta 57, 253-272.

Fitzpatrick, E.M., Bartle, K.D., Kubacki, M.L., Jones, J.M., Pourkashanian, M., Ross, A.B., Williams, A., Kubica, K., 2009. The mechanism of the formation of soot and other pollutants during the co-firing of coal and pine wood in a fixed bed combustor. Fuel 88, 2409-2417.

Ghaly, A.E., Ergüdenler, A., Al Taweel, A.M., 1993. Determination of the kinetic parameters of oat straw using thermogravimetric analysis. Biomass Bioenerg. 5, 457-465.

Haykırı-Açma, H., 2003. Combustion characteristics of different biomass materials. Energ. Convers. Manage. 44, 155-162.

Haykiri-Acma, H., Yaman, S., 2008. Effect of co-combustion on the burnout of lignite/biomasa blends: A Turkish case study. Waste Manage. 28, 2077-2084.

Heikkinen, J.M., Hordijk, J.C., De Jong, W., Splithoff, H., 2004. Thermogravimetry as a tool to classify waste components to be used for energy generation. J. Anal. Appl. Pyrol. 71, 883-900.

Kastanaki, E., Vamvuka, D., 2006. A comparative reactivity and kinetic study on the combustion of coal-biomass char blends. Fuel 85, 1186-1193.

Kastanaki, E., Vamvuka, D., Grammelis, P., Kakaras, E., 2002. Thermogravimetric studies of the behavior of lignite-biomass blends during devolatilization. Fuel Process. Technol. 77-78, 159-166.

Lázaro, M.J., Moliner, R., Suelves, I., 1998. Non-isothermal versus isothermal technique to evaluate kinetic parameters of coal pyrolysis. J. Anal. Appl. Pyrol. 47, 111-125.

Liu, N.A., Fan, W., Dobashi, R., Huang, L., 2002. Kinetic modeling of thermal decomposition of natural cellulosic materials in air atmosphere. J. Anal. Appl. Pyrol. 63, 303-325.

López-Fonseca, R., Landa, I., Elizundia, U., Gutiérrez-Ortiz, M.A., González-Velasco, J.R., 2006. Thermokinetic modeling of the combustion of carbonaceous particulate matter. Combust. Flame 144, 398-406.

McKendry, P., 2002. Energy production from biomass (part 1): overview of biomass. Bioresource Technol. 83, 37-46.

Munir, S., Daood, S.S., Nimmo, W., Cunliffe, A.M., Gibbs, B.M., 2009. Thermal analysis and devolatilization kinetics of cotton stalk, sugar cane bagasse and shea meal under nitrogen and air atmospheres. Bioresource Technol. 100, 1413-1418.

Pis, J.J., de la Puente, G., Fuente, E., Morán, A., Rubiera F., 1996. A study of the self-heating of fresh and oxidized coals by differential thermal análisis. Thermochim. Acta 279, 93-101.

Rubiera, F., Morán, A., Martínez, O., Fuente, E., Pis, J.J., 1997. Influence of biological desulphurisation on coal combustion performance. Fuel Process. Technol. 52, 165-173.

Rubiera, F., Arenillas, A., Fuente, E., Miles, N., Pis, J.J., 1999. Effect of the grinding behaviour of coal blends on coal utilisation for combustion. Powder Technol. 105, 351-356.

Rubiera, F., Arenillas, A., Arias, B., Pis, J.J., 2002. Modification of combustion behaviour and NO emissions by coal blending. Fuel Process. Technol. 77-78, 111-117

Sadhukhan, A.K., Gupta, P., Goyal, T., Saha, R.K., 2008. Modelling of pyrolysis of coal-biomass blends using thermogravimetric analysis. Bioresource Technol. 99, 8022-8026.

Safi, M.J., Mishra, I.M., Prasad, B., 2004. Global degradation kinetics of pine needles in air. Thermochim. Acta 412, 155-162.

Shen, D.K., Gu, S., Luo, K.H., Bridgwater, A.V., Fang, M.X., 2009. Kinetic study on thermal decomposition of woods in oxidative environment. Fuel 88, 1024-1030.

Skodras, G., Grammelis, P., Basinas, P., 2007. Pyrolysis and combustion behaviour of coal-MBM blends. Bioresource Technol. 98, 1-8.

Tillman, D.A., 2000. Biomass cofiring: the technology, the experience, the combustion consequences. Biomass Bioenerg. 19, 365-384.

Vamvuka, D., Kakaras, E., Kastanaki, E., Grammelis, P., 2003a. Pyrolysis characteristics and kinetics of biomass residuals mixtures with lignite. Fuel 82, 1949-1960.

Vamvuka, D., Pasadakis, N., Kastanaki, E., Grammelis, P., Kakaras, E., 2003b. Kinetic modeling of coal/agricultural by-product blends. Energ. Fuel. 17, 549-558.

Wang, C., Wang, F., Yang, Q., Liang, R., 2009. Thermogravimetric studies of the behavior of wheat straw with added coal during combustion. Biomass Bioenerg. 33, 50-56.

Yorulmaz, S.Y., Atimtay, A.T., 2009. Investigation of combustion kinetics of treated and untreated waste wood samples with thermogravimetric analysis. Fuel Process. Technol. 90, 939-946.

Zheng, J.A., Koziński, J.A., 2000. Thermal events occurring during the combustion of biomass residue. Fuel 79, 181-192.

Zhou, L., Wang, Y., Huang, Q., Cai, J., 2006. Thermogravimetric characteristics and kinetic of plastic and biomass blends co-pyrolysis. Fuel Process. Technol. 87, 963-969.

Figure captions

Fig. 1. Experimental and calculated DTG curves for biomass (100P), coal (100C) and blends (5P95C to 80P20C) in an air flow of 50 cm^3 min^{-1}, at a heating rate of 15 ºC min^{-1}.

Fig. 2. Plots of $\ln[g(x)/T^2]$ against $1/T$ that gave the highest correlation coefficient values for all samples.

Table 1
Ultimate and proximate analyses and HHV of the samples

Sample	Ultimate analysis (wt%, db)					Proximate analysis (wt%, db)			HHV (MJ/kg, db)
	C (%)	H (%)	N (%)	O[a] (%)	S (%)	Ash (%)	FC[a] (%)	VM (%)	
Coal (100C)	69.3	4.2	1.8	8.9	0.8	15.0	55.1	29.9	27.8
Pine (100P)	44.1	5.9	0.7	45.5	0.0	3.8	16.4	79.8	18.9

[a] Calculated by difference; db: dry basis

Table 2
Expressions of *g(x)* for the kinetic model functions usually employed for the solid state reactions

Mechanism and model	*g(x)*
Reaction order	
O1	$-\ln(1-x)$
O2	$(1-x)^{-1}$
O3	$(1-x)^{-2}$
Phase boundary controlled reaction	
R2	$1-(1-x)^{1/2}$
R3	$1-(1-x)^{1/3}$
Diffusion	
D1	x^2
D2	$(1-x)\ln(1-x)+x$
D3	$[1-(1-x)^{1/3}]^2$
D4	$1-2x/3-(1-x)^{2/3}$

Table 3
Temperature interval for different regions after loss of moisture, mass loss in these regions, and residues for all samples

Sample	Temperature interval (ºC)			Weight loss (%)			
	Stage B	Stage C	Stage D	Stage B	Stage C	Stage D	Residue (%)
100C	---	---	316-615	---	---	82.8	15.7
5P95C	290-343	343-477	477-616	2.1	27.8	52.3	15.5
10P90C	273-353	353-481	481-617	4.6	28.6	48.8	15.3
20P80C	240-360	360-481	481-616	14.4	26.8	42.7	12.7
50P50C	215-365	365-487	487-606	34.4	26.9	23.4	10.3
80P20C	198-363	363-494	494-595	49.7	27.2	9.4	7.2
100P	196-364	364-487	---	63.9	25.1	---	3.2

C = coal, P = pine.

Table 4
Peak temperature and maximum rate of mass loss for all samples

Sample	Peak temperature (ºC)			Maximum rate of mass loss (% min^{-1})		
	Stage B	Stage C	Stage D	Stage B	Stage C	Stage D
100C	---	---	507	---	---	13.6
5P95C	326	467	508	1.0	8.5	13.2
10P90C	323	467	507	1.7	8.5	12.4
20P80C	323	464	510	4.7	6.9	10.5
50P50C	323	464	510	10.6	5.6	5.8
80P20C	323	454	510	15.2	5.1	2.6
100P	323	447	---	20.1	5.5	---

C = coal, P = pine.

Table 5
Thermal kinetic results of all samples

Sample	Stage B			Stage C			Stage D		
	E (kJ mol^{-1})	A (min^{-1})	R^2	E (kJ mol^{-1})	A (min^{-1})	R^2	E (kJ mol^{-1})	A (min^{-1})	R^2
Model O1									
100C	---	---	---				97.9	9.9E+05	0.9986
5P95C	227.1	6.5E+19	0.9973				115.8	1.2E+07	0.9934
10P90C	149.5	7.4E+12	0.9987				120.2	2.4E+07	0.9928
20P80C	111.4	3.6E+09	0.9978				120.0	2.2E+07	0.9921
50P50C	103.2	7.4E+08	0.9977				134.6	2.0E+08	0.9924
80P20C	102.0	6.1E+08	0.9981				157.0	6.1E+09	0.9936
100P	102.3	6.6E+08	0.9983				---	---	---
Model D3									
100C				---	---	---			
5P95C				228.1	8.7E+14	0.9980			
10P90C				238.6	4.4E+15	0.9981			
20P80C				238.4	5.2E+15	0.9988			
50P50C				224.1	6.3E+14	0.9986			
80P20C				217.4	3.2E+14	0.9983			
100P				236.1	1.5E+16	0.9986			
Model D4									
100C				---	---	---			
5P95C				223.1	5.6E+14	0.9980			
10P90C				229.2	1.2E+15	0.9988			
20P80C				229.5	1.4E+15	0.9992			
50P50C				208.1	4.3E+13	0.9982			
80P20C				195.5	9.4E+12	0.9993			
100P				219.0	6.0E+14	0.9983			

C = coal, P = pine.

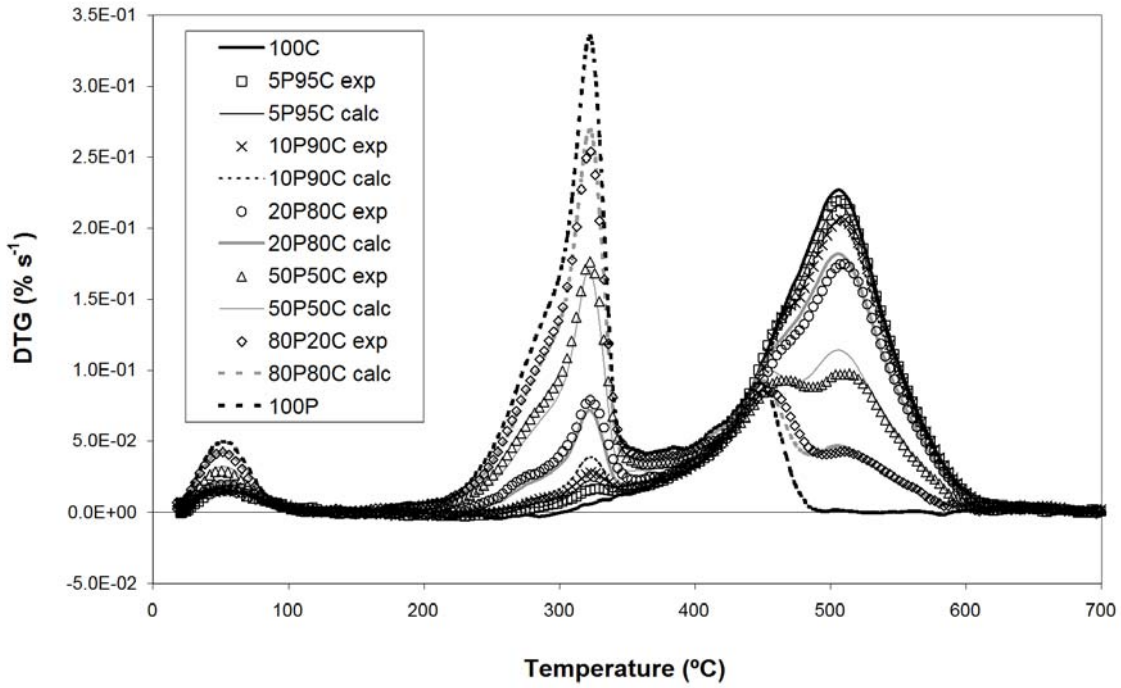
3.5E-01
3.0E-01
2.5E-01
2.0E-01
1.5E-01
1.0E-01
5.0E-02
0.0E+00
-5.0E-02
DTG (% s-1)
0
100
200
300
400
500
600
700
Temperature (ºC)
100C
5P95C exp
5P95C calc
10P90C exp
10P90C calc
20P80C exp
20P80C calc
50P50C exp
50P50C calc
80P20C exp
80P80C calc
100P

Fig. 1.

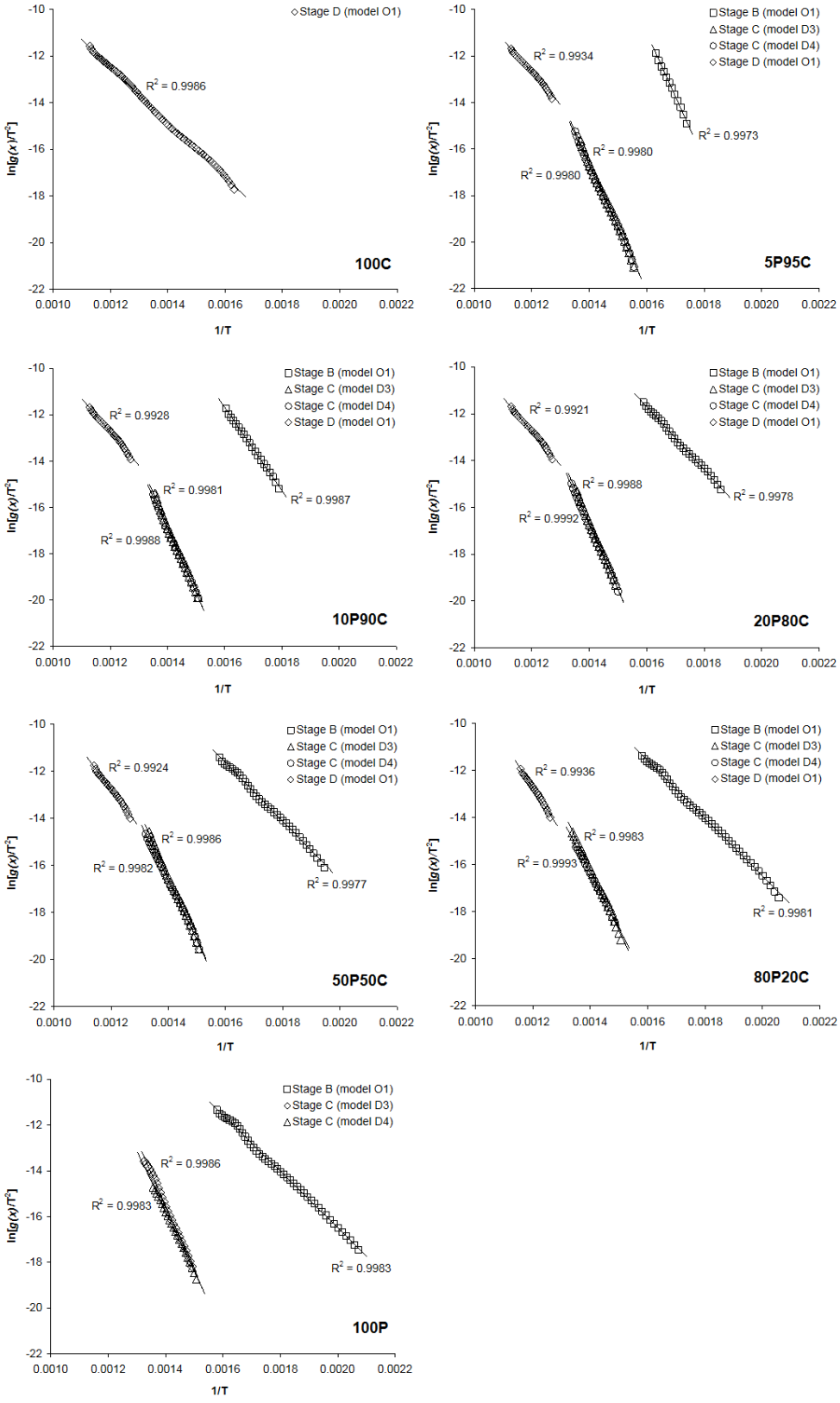
Stage D (model O1)
R² = 0.9986
100C
Stage B (model O1)
Stage C (model D3)
Stage C (model D4)
Stage D (model O1)
R² = 0.9934
R² = 0.9973
R² = 0.9980
R² = 0.9980
5P95C
R² = 0.9928
R² = 0.9981
R² = 0.9987
R² = 0.9988
10P90C
R² = 0.9921
R² = 0.9988
R² = 0.9978
R² = 0.9992
20P80C
R² = 0.9924
R² = 0.9986
R² = 0.9982
R² = 0.9977
50P50C
R² = 0.9936
R² = 0.9983
R² = 0.9993
R² = 0.9981
80P20C
R² = 0.9986
R² = 0.9983
R² = 0.9983
100P
ln[g(x)/T²]
1/T

Fig. 2.